Published in final edited form as:
Magn Reson Med. 2014 November ; 72(5): 1366–1374. doi:10.1002/mrm.25441.

Oscillating gradient diffusion MRI reveals unique microstructural information in normal and hypoxia-ischemia injured mouse brains

Dan Wu[1], **Lee J. Martin**[2,3], **Frances J. Northington**[4], and **Jiangyang Zhang**[5]

[1]Department of Biomedical Engineering, Johns Hopkins University School of Medicine, Baltimore, Maryland, USA

[2]Department of Neuroscience, Johns Hopkins University School of Medicine, Baltimore, Maryland, USA

[3]Department of Pathology, Johns Hopkins University School of Medicine, Baltimore, Maryland, USA

[4]Department of Pediatrics, Johns Hopkins University School of Medicine, Baltimore, Maryland, USA

[5]Department of Radiology, Johns Hopkins University School of Medicine, Baltimore, Maryland, USA

Abstract

Purpose—We investigated whether oscillating gradient diffusion MRI (dMRI) can provide information on brain microstructural changes after formaldehyde fixation and after hypoxic-ischemic (HI) injury beyond that provided by conventional dMRI.

Methods—Pulsed gradient spin echo (PGSE) and oscillating gradient spin echo (OGSE) dMRI of the adult mouse brain was performed in vivo (50-200 Hz, b = 600 mm^2/s), and a similar protocol was applied to neonatal mouse brains at 24 hours after unilateral hypoxia-ischemia. Animals were perfusion fixed with 4% paraformaldehyde for ex vivo dMRI and histology.

Results—Apparent diffusion coefficients (ADCs) measured in the live adult mouse brain presented tissue-dependent frequency-dependence. In vivo OGSE-ADC maps at high oscillating frequencies (>100Hz) showed clear contrast between the molecular layer and granule cell layer in the adult mouse cerebellum. Formaldehyde fixation significantly altered the temporal diffusion spectra in several brain regions. In neonatal mouse brains with HI injury, in vivo ADC measurements from edema regions showed diminished edema contrasts at 200 Hz compared to the PGSE results. Histology showed severe tissue swelling and necrosis in the edema regions.

Conclusion—The results demonstrate the unique ability of OGSE-dMRI in delineating tissue microstructures at different spatial scales.

Correspondence to: Jiangyang Zhang, Ph.D., Traylor Building, Room#208, Johns Hopkins University School of Medicine, 720 Rutland Avenue, Baltimore, MD 21205, USA, jzhang3@jhmi.edu, Phone: (410) 502-9856, Fax: (410) 614-1948.

Keywords

diffusion MRI; oscillating gradient; mouse brain; tissue microstructure; neonatal hypoxia-ischemia

INTRODUCTION

Diffusion MRI (dMRI) utilizes the diffusion of water molecules to exam brain microstructure and is an important tool to visualize brain structures and a wide spectrum of pathologies. Information on the extent of water molecule diffusion in the labyrinth of tissue microstructures is encoded into dMRI signals by diffusion sensitizing gradients (1). By varying the orientation, strength, and timing of the diffusion sensitizing gradients, many aspects of tissue microstructural organization can be extracted from the collected dMRI signals. Advanced dMRI techniques, e.g., high angular resolution diffusion imaging (HARDI) (2,3) and diffusion spectrum imaging (DSI) (4), use sophisticated diffusion encoding schemes with multiple gradient orientations and strengths to reveal the structural organization and connectivity in the brain.

The timing of the diffusion sensitizing gradients, especially the diffusion time, can also be used to explore tissue microstructural properties. The concept of diffusion time dependent dMRI was introduced more than two decades ago (5), and several reports demonstrated diffusion time dependence of dMRI signals in biological tissues (6-9). In order to overcome the limited minimum diffusion time (> 5 ms) in conventional pulsed gradient spin echo (PGSE) methods, oscillating gradient spin echo (OGSE) method was developed to achieve ultra-short diffusion times using high frequency oscillating gradient waveforms (10-14). In fact, OGSE dMRI is a unique tool to measure the so-called temporal diffusion spectrum, which is the Fourier transform of water molecule velocity autocorrelation function (5,15). The relationship between temporal diffusion spectrum and microstructural properties, such as cell size and membrane permeability, has been studied using numerical simulation (16-18) as well as in phantoms (10,19,20) and animals (11,21). Applications of OGSE dMRI to study tissue microstructure in normal (22-27) and diseased brains (28,29) showed promising results. Recently, the feasibility of performing OGSE-dMRI experiments on clinical scanners with limited gradient strengths has been demonstrated, and increased ADCs with oscillating frequency was reported in several white and gray matter structures in the human brain (30,31).

In this study, we further investigated whether OGSE dMRI could provide additional information on brain microstructural changes after formaldehyde fixation and after hypoxic-ischemic injury in the mouse brain. Previous PGSE-dMRI based studies showed significant differences between in vivo and ex vivo ADC values in the brain, as death and chemical fixation can alter tissue microstructural properties, for instance, membrane permeability and relative sizes of tissue compartments (32,33). Similarly, microstructural changes in the brain after hypoxia-ischemia, including swelling of cell bodies and processes, have also been studied (34-36), and such changes may be the underling causes of the dramatic reduction in ADC after acute HI injury (37-39). Understanding how these microstructural changes affect

OGSE-dMRI signals and temporal diffusion spectra will extend our knowledge on the relationships between tissue microstructures and dMRI signals.

METHODS

Animals and experimental setup

In this study, we used five adult C57BL/6 mice (six-month old, female) and 23 postnatal day 10 (P10) C57BL/6 mouse pups (Jackson Laboratory, Bar Harbor, ME, USA). The P10 mouse pups were subjected to hypoxia-ischemia (HI) using the Vannucci model adapted for neonatal mice as described previously (unilateral ligation of the right carotid artery followed by 45 minutes of hypoxia, FiO2=0.08) (40,41). After imaging experiments, mice were sacrificed via transcardially perfusion and fixation with 4% paraformaldehyde (PFA) in phosphate buffered saline (PBS) The mouse heads were then removed and immersed in 4% PFA in PBS for 24 hours to ensure proper fixation. The samples were then washed in PBS and stored at 4 °C in PBS for one week before *ex vivo* MRI. All animal procedures were approved by the Animal Use and Care Committee at the Johns Hopkins University School of Medicine.

Pulse sequences

A PGSE echo planer imaging (EPI) sequence was used to acquire the baseline PGSE MRI data. For the OGSE experiments, the gradient pulses in the PGSE-EPI sequence were replaced by the apodized cosine (11) and cosine-trapezoid (31) oscillating gradient waveforms. In these waveforms, an oscillating period refers to a full cosine period, and only integral numbers of periods were used in this study. The effective b-values of the three sequences were calculated by numerical integration of following equation.

$$b=\int_{-\infty}^{\infty}\left(\int_{0}^{t}g\left(\tau\right)d\tau\right)^{2}dt \quad \text{Equation 1}$$

The calculation of effective b-values was validated using an agarose gel (4% by weight) phantom with a b-value of 600 s/mm^2. No statistical difference in ADC measurements was found among the PGSE, apodized cosine, and cosine-trapezoid OGSE at 50 Hz to 200 Hz.

In vivo MRI of the adult and neonatal mouse brain

In vivo MRI experiments were performed on a horizontal 11.7 Tesla Bruker scanner (Bruker Biospin, Billerica, MA, USA) with a B-GA 9S gradient system (maximum gradient strength = 740 mT/m, maximum slew rate = 6,600 T/m/s). During imaging, mice were anesthetized with isoflurane (1%) together with air and oxygen mixed at 3:1 ratio via a vaporizer. Two 4% agarose gel phantoms were placed on both sides of the brain for calibration. OGSE-dMRI was acquired using the cosine-trapezoid oscillating gradient waveform and 4-segment multi-slice EPI readout with a partial Fourier factor of 1.32 and respiration triggering. The maximum gradient and slew rate used at 200 Hz were 455 mT/m and 3,640 T/m/s per channel.

OGSE-dMRI of the adult mouse forebrain was performed using a 72 mm volume transmit coil and a 15 mm planar surface receive coil with the following parameters: echo time (TE)/

repetition time (TR) = 57.5/5000 ms; four signal average; diffusion gradient length (δ) = 20 ms; number of oscillating periods (N) = 1, 2, 3, 4 for oscillating frequencies of 50Hz, 100Hz, 150Hz and 200Hz, respectively; b-value = 600 s/mm^2; two non-diffusion weighted images (b_0 images) and six diffusion weighted images (gradient directions: [1/1/0], [1/0/1], [0/1/1], [−1/1/0], [1/0/−1], [0/−1/1]); 0.125×0.125 mm^2 in-plane resolution with a field of view (FOV) of 16×16 mm^2; eight 0.8 mm thick coronal slices; scan time ≈ 11 minutes for each oscillating frequency.

OGSE-dMRI of the HI-injured neonatal mouse brain was performed at 24 hours after hypoxic ischemic injury (P11) using a 72 mm volume transmit coil and a 10 mm planar surface receive coil with the same parameters as used for the adult mouse forebrain except: TE/TR = 52/2000 ms; in-plane resolution = 0.17×0.17 mm^2; scan time ≈ 5 minutes for each oscillating frequency.

The mouse cerebellum was imaged using a quadrature surface transmit/receive cryogenic probe (42) with slightly different parameters: TE/TR = 44/2000 ms; eight signal average; δ = 15 ms; N = 2, 3, 4 for oscillating frequencies of 100Hz, 150Hz, and 200Hz, respectively; b-value = 600 s/mm2; two b_0 images and ten diffusion weighted images (the six directions listed previously plus [1/1/1], [−1/1/1], [1/−1/1], [1/1/−1]); 0.1×0.1 mm^2 in-plane resolution with a FOV of 12.8×9.6 mm^2; six 0.6 mm thick sagittal slices; scan time ≈ 13 minutes for each oscillating frequency.

PGSE data were acquired with the same parameters (including TE and TR) as the corresponding OGSE data, except δ/diffusion separation (Δ) = 4/20 ms. Co-registered T2-weighted images were acquired using a fast spin echo sequence with TE/TR = 50/3000 ms, two signal averages, and echo train length = 8. The signal-to-noise ratios (SNRs), calculated as the ratio between the mean signal intensity of the specified region and standard deviation of the background noise in the b_0 images, were greater than 50 in the cortex for both OGSE and PGSE experiments.

Ex vivo MRI

Ex vivo dMRI of the same adult and P11 mouse brains was performed on a vertical 17.6 Tesla NMR spectrometer (Bruker Biospin, Billerica, MA, USA) with a Micro2.5 gradient system (maximum gradient strength = 1500 mT/m) and a 15 mm diameter transceiver volume coil. During MRI, the specimens were immersed in fomblin (Fomblin Perfluoropolyether, Solvay Solexis, Thorofare, NJ, USA) for susceptibility matching and to prevent dehydration. The temperature of the specimens was maintained at 37 °C via the spectrometer's temperature control system. The same imaging protocol as the *in vivo* MRI was used, except that a higher b-value (800 s/mm^2) was used to compensate for the reduced ADC in the ex vivo brains. The SNR measured in the cortex were greater than 70 for both OGSE and PGSE experiments.

Data analysis

The ADC maps were calculated by averaging the diffusion coefficients from the all diffusion directions with ADC = $-\ln(S/S_0)/(b\text{-}b_0)$. ADC values from in vivo experiments

were corrected based on the ADCs of the agarose gel phantoms. The rate of ADC increase with oscillating frequency (Δ*f*ADC) was calculated by the linear fitting in Matlab (www.mathworks.com). The regions of interest (ROIs) were manually defined using ROIEditor (www.mristudio.org) for quantitative analysis. In the HI-injured neonatal mouse brains, ROIs were placed in the core of cortical and hippocampal edema defined by reduced PGSE-ADC values and matching locations on the contralateral side, based on which the group mean and inter-subject standard deviation were determined. Paired two-tailed Student's t-tests were performed between the in vivo and ex vivo measurements from the adult mouse brains (n=5), and between the ipsilateral and contralateral regions in the neonatal HI mouse brains (n=6) using Microsoft Excel.

Tissue processing and histopathology

Perfusion fixed mouse brains were removed from skulls and cryo-protected in 30% sucrose. The brains were cut serially on a sliding microtome at a thickness of 80 microns. Every 10th section was stained with cresyl-violet and adjacent sections were stained with hematoxylin and eosin (H&E). Near-adjacent sections were stained immunohistochemically for glial fibrillary and acidic protein (GFAP). An immunoperoxidase method was used with a polyclonal rabbit antibody (Dako, Carpinteria, CA) to GFAP at a dilution of 1:2000. Immunoreactivity was visualized using affinity purified goat anti-rabbit secondary antibody, rabbit peroxidase-antiperoxidase, and diaminobenzedine as chromogen. The histological slides were imaged with a Nikon microscope (Nikon Instruments Inc., Melville, NY, USA) and a ProgRes C14 Plus digital camera (Jenoptik, Rochester, NY).

RESULTS

Formaldehyde fixation altered the temporal diffusion spectra in the adult mouse brain

Both in vivo and ex vivo OGSE-dMRI of the adult mouse brain showed frequency-dependent ADC changes (Fig. 1). In the cortex and hippocampus, the rates at which the in vivo ADC values increased with frequencies (Δ*f*ADC) were 0.33 ± 0.05 μm^2 and 0.38 ± 0.05 μm^2, respectively (Table 1). In comparison, ex vivo PGSE-ADC values measured in the same regions were significantly reduced. With increasing frequency, the ex vivo OGSE-ADC values in the cortex and hippocampus increased more rapidly than the in vivo measurements, and the corresponding Δ*f*ADC values (Table 1) were significantly higher than the in vivo estimates ($p = 8.85 \times 10^{-7}$ and $p = 2.57 \times 10^{-6}$). As a result, the differences between in vivo and ex vivo OGSE-ADC values gradually decreased in the cortex (Fig. 1B) and hippocampus (Fig. 1C) with increasing frequency.

In the mouse cerebellum, we also found considerable differences between the in vivo and ex vivo temporal diffusion spectra. The in vivo ADC values in the cerebellar granule cell layer (CBGr) and cerebellar molecular layer (CBML) were significantly higher (1.5-2 times) than the ex vivo ADC values in PGSE and OGSE up to 200 Hz (Fig. 2A-B). The in vivo Δ*f*ADC of the CBGr (3.46 ± 0.21 μm^2) was significantly higher than the ex vivo values (2.21 ± 0.20 μm^2, $p = 1.11 \times 10^{-5}$, Fig. 2C). No significant difference was found between the in vivo and ex vivo Δ*f*ADC values in the CBML ($p = 0.32$, Fig. 2C). These differences resulted in

different contrasts between CBGr and CBML in the in vivo and ex vivo ADC maps over the 0-200 Hz frequency range (Fig. 2A).

Pseudo-normalization of OGSE-ADC values observed in severe edema regions after neonatal HI injury

Among the twenty-three neonatal mice that underwent right carotid artery ligation and hypoxia, six mice (three males and three females) developed extensive cortical and hippocampal edema on the ligated side at 24 hours after injury. The other mice either exhibited no MRI-visible injury or mild injury in regions other than the cortex and hippocampus. The extensive edema in the six mice was marked by reduced PGSE-ADC and hyper-intense T2 signals (Fig. 3). The PGSE-ADCs in the ipsilateral cortex and hippocampus were reduced by 51.9 ± 5.4% and 42.3 ± 8.7% with respect to the contralateral side, respectively (Fig. 4B-C, Table 2). As frequency increases, the contrast between the edema regions and neighboring regions gradually decreased in the OGSE-ADC maps compared to the PGSE results. The pseudo-normalization of OGSE-ADC values in the edema region was the result of rapid increase in OGSE-ADC values with increasing frequency (Fig. 4). For example, the Δ*f*ADC values were elevated by 4.5 times in the ipsilateral cortex compared to its contralateral counterpart, and 3.7 times in hippocampus (Table 2). At 200 Hz, the ipsilateral ADC values became statistically undistinguishable from the contralateral side (Fig. 4B-C). Within the hippocampus, two layer structures (Region 1 and 2 (R1/R2) as defined in Fig. 3) were enhanced in the OGSE-ADC maps at 100-200 Hz and in the Δ*f*ADC map.

Ex vivo dMRI on the same neonatal mouse brains after 4% PFA fixation disclosed large variations in ADC values in the ipsilateral cortex and hippocampus, as indicated by the blue and orange arrows in Fig. 3. Despite the large variability in ex vivo ADC values, the Δ*f*ADC values measured in the ipsilateral cortical and hippocampal lesions remained fairly consistent (1.35 ± 0.08 μm^2), which were significantly higher than those in the contralateral cortex and hippocampus (1.02 ± 0.13 μm^2, $p = 0.002$, more details can be found in supplemental table 1). Ex vivo ADC measurements in the contralateral brain were consistent, which also had elevated Δ*f*ADC values but at a lesser degree compared to that in the edema regions (Fig. 4A-C).

A histological survey of H&E-stained sections revealed severe tissue swelling in the hippocampus (Fig. 5A-B) and cerebral cortex (Fig. 5C-D) at 24hrs of recovery in the P11 mouse brains. In the hippocampus, the CA1 region in HI mice showed discrete expansion of several layers, including the stratum oriens (so), stratum radiatum (sr), and stratum lacunosum-moleculare (slm) (Fig. 5A-B). The slm appeared to have the most severe injury in hippocampus at 24hrs after HI (compare the length of the identified arrows, Fig. 5A-B). Edema was also present in the somatosensory cortex. The damaged zone showed a clear pallor of staining compared to the nearby normal appearing cortical parenchyma (Fig. 5C-D). Cortical swelling was evident by comparing the width between the pial surface and the subcortical white matter (marked by black lines in Fig. 5C-D). GFAP immunostaining revealed activation of astrocytes in hippocampus at 24hrs after HI compared to controls

(Fig. 5E-H). Injured astrocytic processes in HI hippocampus were swollen and appeared fragmented in some instances.

DISCUSSION

An appealing feature of OGSE-dMRI is its potential to filter dMRI signals based on the sizes of underlying microstructural barriers and thereby provide an additional perspective on tissue microstructural organization and integrity. To better understand the capability of OGSE-dMRI, it is important to examine perturbations in temporal diffusion spectra in response to tissue microstructural changes, especially under pathological conditions. In this study, a relatively small portion of the temporal diffusion spectrum was measured in the mouse brain, from 0 Hz (PGSE) to 200 Hz with a spectral resolution of 50 Hz. We measured changes in temporal diffusion spectra using absolute ADC values and Δ*f*ADC, which was simply the slope of ADC increase as the frequency increased from 0 Hz to 200 Hz. The effective diffusion times in this study ranged from 20 ms (PGSE) down to 1.25 ms (OGSE at 200 Hz), during which the mean square distances of water molecule diffusion fell from 11 μm to 2.7 μm (calculated based on the free water diffusion constant of 3×10^{-3} mm^2/s at body temperature (43)). These distances approximate those at the cellular and subcellular level, e.g., the nucleus, and in pathological settings where mitochondrial diameter can approach 5 μm (44,45). Based on the results of previous phantom experiments (10) and simulations (17), this limited frequency span and resolution will only allow us to examine microstructures within a certain range of spatial scales, with reduced sensitivity for microstructures outside this range. The observed temporal diffusion spectra of CBGr and CBML exemplify this property (Fig. 2). The CBML consists of a large number of parallel fibers with diameters approximately 0.2-0.3 μm (46), which is an order of magnitude smaller than the mean square distance of free water diffusion at 200 Hz. This may explain why ADC values in the CBML showed little change from 0 to 200 Hz and little change in Δ*f*ADC values after fixation. In comparison, the CBGr contains densely packed granule cells (5-10 μm in diameter) (47), and there were moderate increases of ADC with increasing frequency and significant differences between its Δ*f*ADC values measured in vivo and ex vivo (Fig. 2B-C).

Comparisons between in vivo and ex vivo OGSE dMRI data demonstrated that formaldehyde fixation significantly alters the temporal diffusion spectra in biological tissues. The slightly higher b-value used in the ex vivo experiments (800 s/mm^2) than the in vivo experiments (600 s/mm^2) should not introduce significant biases in ADC estimates as the signal decays at these b-values were mostly mono-exponential in both PGSE and OGSE experiments (25). The reductions in PGSE-ADCs in formaldehyde fixed mouse cortex and hippocampus are consistent with previous reports (32,33). Narrowing of the gaps between in vivo and ex vivo ADCs as frequency increased and increases in Δ*f*ADCs in cortex and hippocampus (Fig. 1 and Table 1) are also similar to findings by Does et al. (11) in rat brains after global ischemia in the frequency range of 0-500 Hz.

Structural changes that potentially contribute to these changes are multifold, including changes in surface-to-volume ratio, compartment size and diffusivity, cell membrane permeability, and nuclear-to-cell ratio (16,19,20). A previous report on the effects of tissue

fixation on diffusion properties of rat brain slices (32) showed increased intracellular apparent restriction size, likely due to cell swelling (48), after fixation with 4% formaldehyde. According to numerical simulations based on a tissue model of densely packed cells (16), an increase in cell size will lead to increased Δ*f*ADC, which agrees with our observations in the cortex and hippocampus (Fig. 1 and Table 1). As the differences between in vivo and ex vivo OGSE-ADC values remained significant at 200 Hz, additional microstructural changes may exist at the subcellular or lower levels. Previously, we showed that, in ex vivo mouse brains, the CBGr and several other regions with densely populated neuronal cell bodies had significantly higher Δ*f*ADC than other regions (22). In this study, high-resolution in vivo images of the mouse cerebellum also showed a frequency dependent contrast between CBML and CBGr (Fig. 2). It is not clear what caused the drop in Δ*f*ADC by 36% in the CBGr after death and tissue fixation.

Microstructural changes under pathological conditions can provide additional insights into the sensitivity of OGSE-dMRI to tissue microstructures. Previous studies in cat brains after middle cerebral artery occlusion showed no diffusion time dependence in ADC for diffusion times from 20 ms to 2 s (49). In the neonatal mouse model of unilateral hypoxic-ischemia (29,40), we found significant diffusion time dependence at diffusion times from 1.25 ms to 20 ms. The pseudo-normalization of OGSE-ADC values in the edema region agree with a recent human acute stroke study by Baron et al (50), in which the authors related their findings to white matter beading and swelling. The phenomenon suggests that the microstructural changes associated with the decrease in PGSE-ADC are mostly at the cellular or subcellular level (> 2 μm), e.g., swelling of cells, as suggested by previous reports (37) and consistent with our histological assessments.

As discussed above, multiple microstructural changes can lead to the change in temporal diffusion spectra in the edema regions. It is known that, in cytotoxic edema shortly after hypoxic-ischemia, energy failure of the ion channels causes an influx of water from extracellular space to the intracellular space (54). The expansion of the affected cortex and hippocampal layers, which resulted from tissue swelling as shown in our histological data, was likely an important factor accounting for the drop in PGSE-ADC and increases in Δ*f*ADC. We also found severe necrosis in the ipsilateral cortex and hippocampus, including break down of the nuclei and cellular organelles, which may also explain the elevated Δ*f*ADC values as the intracellular environment became less restrictive. The locations of the two layer structures in the hippocampus highlighted in the 200 Hz OGSE-ADC maps (R1/R2 in Fig. 3) correlated with the hippocampal pyramidal cell layer, the granule cell layer in the dentate gyrus, and their extended dendritic arborization in neighboring regions. The fact that the two regions showed higher OGSE-ADC values than the contralateral side at 200 Hz suggests there were microstructural changes at subcellular or finer levels.

CONCLUSION

In summary, we found that formaldehyde fixation can significantly alter the temporal diffusion spectra in the mouse brain. The tissue contrast between CBGr and CBML in post-mortem mouse cerebellum could be reproduced in live animals. In the neonatal mouse brain with hypoxic ischemic injury, pseudo-normalization of OGSE-ADCs in the edema regions

suggest that the microstructural changes associated with the decrease in PGSE-ADC are mostly at the cellular or subcellular level.

Supplementary Material

Refer to Web version on PubMed Central for supplementary material.

Acknowledgments

This study was supported by the National Institute of Health grants R01NS070909, R01HD074593, and R01HD070996.

REFERENCES

1. Le Bihan D. Looking into the functional architecture of the brain with diffusion MRI. Nat Rev Neurosci. 2003; 4(6):469–480. [PubMed: 12778119]
2. Frank LR. Anisotropy in high angular resolution diffusion-weighted MRI. Magn Reson Med. 2001; 45(6):935–939. [PubMed: 11378869]
3. Tuch DS, Reese TG, Wiegell MR, Wedeen VJ. Diffusion MRI of complex neural architecture. Neuron. 2003; 40(5):885–895. [PubMed: 14659088]
4. Wedeen VJ, Hagmann P, Tseng WY, Reese TG, Weisskoff RM. Mapping complex tissue architecture with diffusion spectrum magnetic resonance imaging. Magn Reson Med. 2005; 54(6): 1377–1386. [PubMed: 16247738]
5. Stepisnik J. Time-Dependent Self-Diffusion by Nmr Spin-Echo. Physica B. 1993; 183(4):343–350.
6. Helmer KG, Dardzinski BJ, Sotak CH. The application of porous-media theory to the investigation of time-dependent diffusion in in vivo systems. NMR in biomedicine. 1995; 8(7-8):297–306. [PubMed: 8739268]
7. Niendorf T, Norris DG, Leibfritz D. Detection of Apparent Restricted Diffusion in Healthy Rat-Brain at Short Diffusion Times. Magnet Reson Med. 1994; 32(5):672–677.
8. Moonen CTW, Pekar J, Devleeschouwer MHM, Vangelderen P, Vanzijl PCM, Despres D. Restricted and Anisotropic Displacement of Water in Healthy Cat Brain and in Stroke Studied by Nmr Diffusion Imaging. Magnet Reson Med. 1991; 19(2):327–332.
9. Clark CA, Hedehus M, Moseley ME. Diffusion time dependence of the apparent diffusion tensor in healthy human brain and white matter disease. Magnet Reson Med. 2001; 45(6):1126–1129.
10. Parsons EC Jr. Does MD, Gore JC. Temporal diffusion spectroscopy: theory and implementation in restricted systems using oscillating gradients. Magn Reson Med. 2006; 55(1):75–84. [PubMed: 16342147]
11. Does MD, Parsons EC, Gore JC. Oscillating gradient measurements of water diffusion in normal and globally ischemic rat brain. Magn Reson Med. 2003; 49(2):206–215. [PubMed: 12541239]
12. Gore JC, Xu J, Colvin DC, Yankeelov TE, Parsons EC, Does MD. Characterization of tissue structure at varying length scales using temporal diffusion spectroscopy. NMR in biomedicine. 2010; 23(7):745–756. [PubMed: 20677208]
13. Schachter M, Does MD, Anderson AW, Gore JC. Measurements of restricted diffusion using an oscillating gradient spin-echo sequence. J Magn Reson. 2000; 147(2):232–237. [PubMed: 11097814]
14. Ianus A, Siow B, Drobnjak I, Zhang H, Alexander DC. Gaussian phase distribution approximations for oscillating gradient spin echo diffusion MRI. Journal of Magnetic Resonance. 2013; 227:25–34. [PubMed: 23261952]
15. Parsons EC, Does MD, Gore JC. Modified oscillating gradient pulses for direct sampling of the diffusion spectrum suitable for imaging sequences. Magnetic resonance imaging. 2003; 21(3-4): 279–285. [PubMed: 12850719]
16. Xu J, Does MD, Gore JC. Dependence of temporal diffusion spectra on microstructural properties of biological tissues. Magnetic resonance imaging. 2011; 29(3):380–390. [PubMed: 21129880]

17. Xu J, Does MD, Gore JC. Quantitative characterization of tissue microstructure with temporal diffusion spectroscopy. J Magn Reson. 2009; 200(2):189–197. [PubMed: 19616979]
18. Xu J, Does MD, Gore JC. Sensitivity of MR diffusion measurements to variations in intracellular structure: effects of nuclear size. Magn Reson Med. 2009; 61(4):828–833. [PubMed: 19205020]
19. Novikov DS, Kiselev VG. Surface-to-volume ratio with oscillating gradients. Journal of Magnetic Resonance. 2011; 210(1):141–145. [PubMed: 21393035]
20. Portnoy S, Fichtner ND, Dziegielewski C, Stanisz MP, Stanisz GJ. In vitro detection of apoptosis using oscillating and pulsed gradient diffusion magnetic resonance imaging. NMR in biomedicine. 2014; 27(4):371–380. [PubMed: 24421173]
21. Colvin DC, Yankeelov TE, Does MD, Yue Z, Quarles C, Gore JC. New insights into tumor microstructure using temporal diffusion spectroscopy. Cancer Res. 2008; 68(14):5941–5947. [PubMed: 18632649]
22. Aggarwal M, Jones MV, Calabresi PA, Mori S, Zhang J. Probing mouse brain microstructure using oscillating gradient diffusion MRI. Magn Reson Med. 2012; 67(1):98–109. [PubMed: 21590726]
23. Kershaw J, Leuze C, Aoki I, Obata T, Kanno I, Ito H, Yamaguchi Y, Handa H. Systematic changes to the apparent diffusion tensor of in vivo rat brain measured with an oscillating-gradient spin-echo sequence. NeuroImage. 2013; 70:10–20. [PubMed: 23274188]
24. Portnoy S, Flint JJ, Blackband SJ, Stanisz GJ. Oscillating and pulsed gradient diffusion magnetic resonance microscopy over an extended b-value range: implications for the characterization of tissue microstructure. Magn Reson Med. 2013; 69(4):1131–1145. [PubMed: 22576352]
25. Pyatigorskaya N, Le Bihan D, Reynaud O, Ciobanu L. Relationship between the diffusion time and the diffusion MRI signal observed at 17.2 tesla in the healthy rat brain cortex. Magnet Reson Med. 72(2):492–500. 201.
26. Lundell H, Sonderby CK, Dyrby TB. Diffusion weighted imaging with circularly polarized oscillating gradients. Magn Reson Med. 2014 doi: 10.1002/mrm.25211.
27. Siow B, Drobnjak I, Ianus A, Christie IN, Lythgoe MF, Alexander DC. Axon radius estimation with oscillating gradient spin echo (OGSE) diffusion MRI. Diffus Fundam Org. 2013; 18:1–6.
28. Xu J, Li K, Smith RA, Waterton JC, Zhao P, Chen H, Does MD, Manning HC, Gore JC. Characterizing tumor response to chemotherapy at various length scales using temporal diffusion spectroscopy. PloS one. 2012; 7(7):e41714. [PubMed: 22911846]
29. Aggarwal M, Burnsed J, Martin LJ, Northington FJ, Zhang J. Imaging neurodegeneration in the mouse hippocampus after neonatal hypoxia-ischemia using oscillating gradient diffusion MRI. Magn Reson Med. 2013 doi: 10.1002/mrm.24956.
30. Baron CA, Beaulieu C. Oscillating Gradient Spin-Echo (OGSE) diffusion tensor imaging of the human brain. Magn Reson Med. 2013 doi: 10.1002/mrm.24987.
31. Van AT, Holdsworth SJ, Bammer R. In vivo investigation of restricted diffusion in the human brain with optimized oscillating diffusion gradient encoding. Magn Reson Med. 2014; 71(1):83–94. [PubMed: 23447055]
32. Shepherd TM, Thelwall PE, Stanisz GJ, Blackband SJ. Aldehyde fixative solutions alter the water relaxation and diffusion properties of nervous tissue. Magn Reson Med. 2009; 62(1):26–34. [PubMed: 19353660]
33. Sun SW, Neil JJ, Liang HF, He YY, Schmidt RE, Hsu CY, Song SK. Formalin fixation alters water diffusion coefficient magnitude but not anisotropy in infarcted brain. Magn Reson Med. 2005; 53(6):1447–1451. [PubMed: 15906292]
34. Martin LJ, Brambrink AM, Lehmann C, Portera-Cailliau C, Koehler R, Rothstein J, Traystman RJ. Hypoxia-ischemia causes abnormalities in glutamate transporters and death of astroglia and neurons in newborn striatum. Annals of neurology. 1997; 42(3):335–348. [PubMed: 9307255]
35. Northington FJ, Ferriero DM, Graham EM, Traystman RJ, Martin LJ. Early Neurodegeneration after Hypoxia-Ischemia in Neonatal Rat Is Necrosis while Delayed Neuronal Death Is Apoptosis. Neurobiology of disease. 2001; 8(2):207–219. [PubMed: 11300718]
36. Vannucci RC, Vannucci SJ. Perinatal hypoxic-ischemic brain damage: evolution of an animal model. Developmental neuroscience. 2005; 27(2-4):81–86. [PubMed: 16046840]
37. Sotak CH. The role of diffusion tensor imaging in the evaluation of ischemic brain injury - a review. NMR in biomedicine. 2002; 15(7-8):561–569. [PubMed: 12489102]

38. Sizonenko SV, Camm EJ, Garbow JR, Maier SE, Inder TE, Williams CE, Neil JJ, Huppi PS. Developmental changes and injury induced disruption of the radial organization of the cortex in the immature rat brain revealed by in vivo diffusion tensor MRI. Cerebral cortex. 2007; 17(11): 2609–2617. [PubMed: 17259644]
39. Chan KC, Khong PL, Lau HF, Cheung PT, Wu EX. Late measures of microstructural alterations in severe neonatal hypoxic-ischemic encephalopathy by MR diffusion tensor imaging. International journal of developmental neuroscience. 2009; 27(6):607–615. [PubMed: 19505567]
40. Rice JE 3rd, Vannucci RC, Brierley JB. The influence of immaturity on hypoxic-ischemic brain damage in the rat. Annals of neurology. 1981; 9(2):131–141. [PubMed: 7235629]
41. Ditelberg JS, Sheldon RA, Epstein CJ, Ferriero DM. Brain injury after perinatal hypoxia-ischemia is exacerbated in copper/zinc superoxide dismutase transgenic mice. Pediatr Res. 1996; 39(2):204–208. [PubMed: 8825788]
42. Baltes C, Radzwill N, Bosshard S, Marek D, Rudin M. Micro MRI of the mouse brain using a novel 400 MHz cryogenic quadrature RF probe. NMR in biomedicine. 2009; 22(8):834–842. [PubMed: 19536757]
43. Simpson JH, Carr HY. Diffusion and Nuclear Spin Relaxation in Water. Phys Rev. 1958; 111(5): 1201–1202.
44. Martin LJ, Liu Z, Chen K, Price AC, Pan Y, Swaby JA, Golden WC. Motor neuron degeneration in amyotrophic lateral sclerosis mutant superoxide dismutase-1 transgenic mice: mechanisms of mitochondriopathy and cell death. The Journal of comparative neurology. 2007; 500(1):20–46. [PubMed: 17099894]
45. Martin LJ, Gertz B, Pan Y, Price AC, Molkentin JD, Chang Q. The mitochondrial permeability transition pore in motor neurons: involvement in the pathobiology of ALS mice. Experimental neurology. 2009; 218(2):333–346. [PubMed: 19272377]
46. Wyatt KD, Tanapat P, Wang SSH. Speed limits in the cerebellum: constraints from myelinated and unmyelinated parallel fibers. Eur J Neurosci. 2005; 21(8):2285–2290. [PubMed: 15869526]
47. Sillitoe, RV.; Fu, Y.; Watson, C. Cerebellum. In: Watson, C.; Paxinos, G.; Puelles, L., editors. The Mouse Nervous System. Academic Press; New York: 2012. p. 360-397.
48. Grawford GNC, Barer R. The action of Formaldehyde on living cells as studied by phase-contrast microscopy. Quarterly Journal of Microscopical Science. 1951; 92(4):403–452.
49. van Gelderen P, de Vleeschouwer MH, DesPres D, Pekar J, van Zijl PC, Moonen CT. Water diffusion and acute stroke. Magn Reson Med. 1994; 31(2):154–163. [PubMed: 8133751]
50. Baron, CA.; Kate, M.; Gioia, LC.; Butcher, K.; Emery, D.; Budde, MD.; Beaulieu, C. Oscillating Gradient Spin-Echo (OGSE) DTI Yields Mechanistic Insights in Human Stroke; In Proceedings of the 22th Annual Meeting of ISMRM; Milano, Italy. 2014; p. 0106
51. van der Toorn A, Dijkhuizen RM, Tulleken CA, Nicolay K. Diffusion of metabolites in normal and ischemic rat brain measured by localized 1H MRS. Magn Reson Med. 1996; 36(6):914–922. [PubMed: 8946357]
52. Wick M, Nagatomo Y, Prielmeier F, Frahm J. Alteration of intracellular metabolite diffusion in rat brain in vivo during ischemia and reperfusion. Stroke. 1995; 26(10):1930–1933. discussion 1934. [PubMed: 7570750]
53. Ackerman JJH, Neil JJ. The use of MR-detectable reporter molecules and ions to evaluate diffusion in normal and ischemic brain. NMR in biomedicine. 2010; 23(7):725–733. [PubMed: 20669147]
54. Qiao M, Malisza KL, Del Bigio MR, Tuor UI. Transient hypoxia-ischemia in rats: changes in diffusion-sensitive MR imaging findings, extracellular space, and Na+-K+ -adenosine triphosphatase and cytochrome oxidase activity. Radiology. 2002; 223(1):65–75. [PubMed: 11930049]

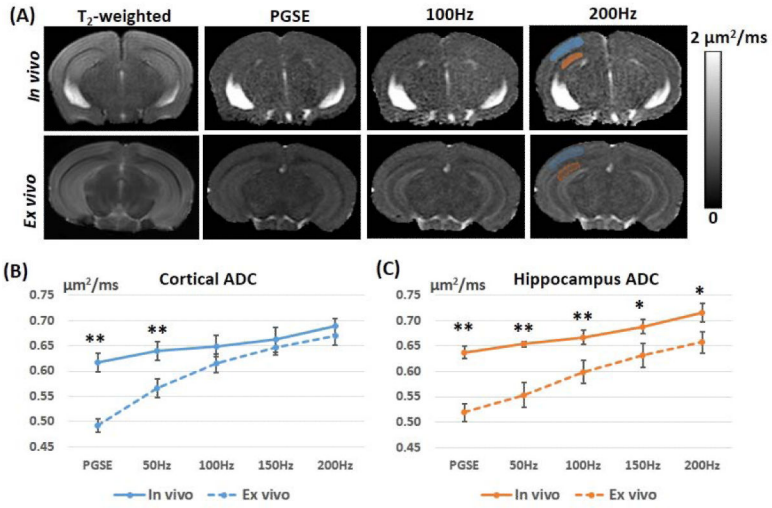

Fig. 1.

Comparisons of in vivo and ex vivo ADC maps of the adult mouse brain acquired using pulsed gradient spin echo (PGSE) and oscillating gradient spin echo (OGSE) methods. A: Axial T2-weighted, PGSE-ADC, and OGSE-ADC (at 100 and 200 Hz) images of a representative adult mouse brain. The blue and red shadings indicate the regions of interest that are manually placed to obtain ADC values in the cortex and hippocampus, respectively. B-C: Plots of in vivo ADC (solid lines) and ex vivo ADC (dashed lines) values measured in the cortex and hippocampus at different frequencies (n = 5). Error bars indicate the inter-subject standard deviation. * and ** denote that a two-tailed t-test between the in vivo and ex vivo measurements produced a *p*-value less than 0.01 and 0.001, respectively.

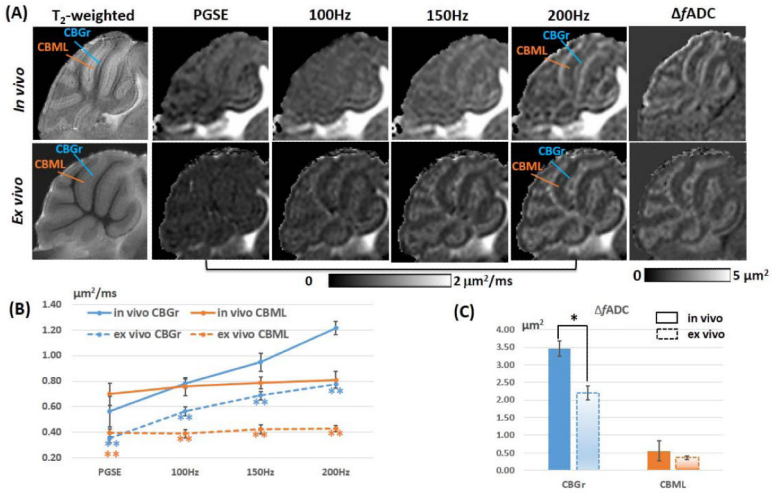

Fig. 2.

Frequency-dependent tissue contrast in the adult mouse cerebellum. A: Para-sagittal (0.6 mm off the midline) T2-weighted, PGSE-ADC, OGSE-ADC, and fitted Δ*f*ADC images of the in vivo and ex vivo mouse cerebellum. The orange lines indicate the location of the cerebellar molecular layer (CBML), and the blue lines indicate the location of the cerebellar granule cell layer (CBGr). B: Plots of in vivo and ex vivo ADC values measured in the CBGr and CBML at different frequencies (n = 5). C: Comparison of the in vivo and ex vivo Δ*f*ADC values in the CBGr and CBML (n = 5). Error bars indicate the inter-subject standard deviation. * and ** denote that a two-tailed t-test between the in vivo and ex vivo measurements produced a *p*-value less than 0.05 and 0.001, respectively.

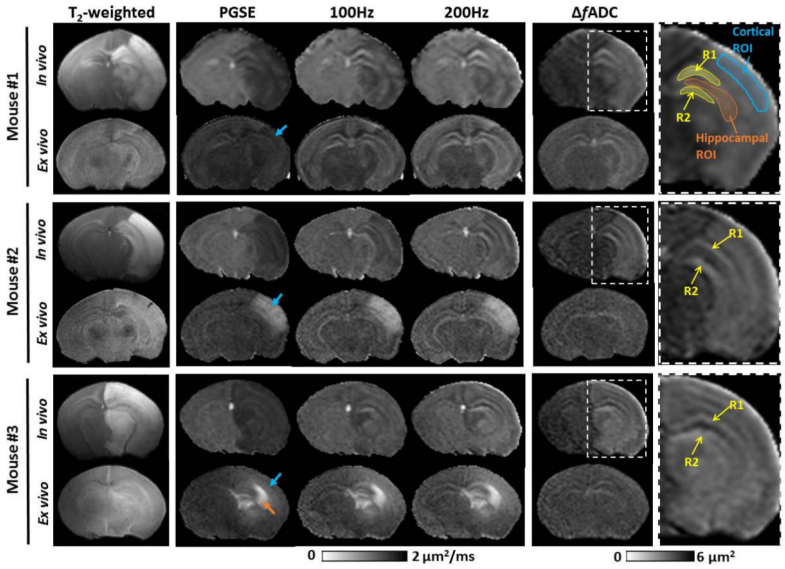

Fig. 3.

Representative MR images of three (out of six) P11 mice with severe edema in the cortex and hippocampus. Axial T2-weighted, PGSE-ADC, OGSE-ADC (at 100 and 200 Hz), and Δ*f*ADC maps were shown. Both in vivo and ex vivo MR images were displayed. The blue and orange arrows indicate high signal variations in the ipsilateral cortical and hippocampal regions of ex vivo specimens, respectively. The yellow arrows indicate two layers (R1/R2) in the ipsilateral hippocampus that were enhanced at 200 Hz. Definitions of the cortical, hippocampal and R1/R2 ROIs were superimposed on the enlarged Δ*f*ADC map of the injured hemisphere.

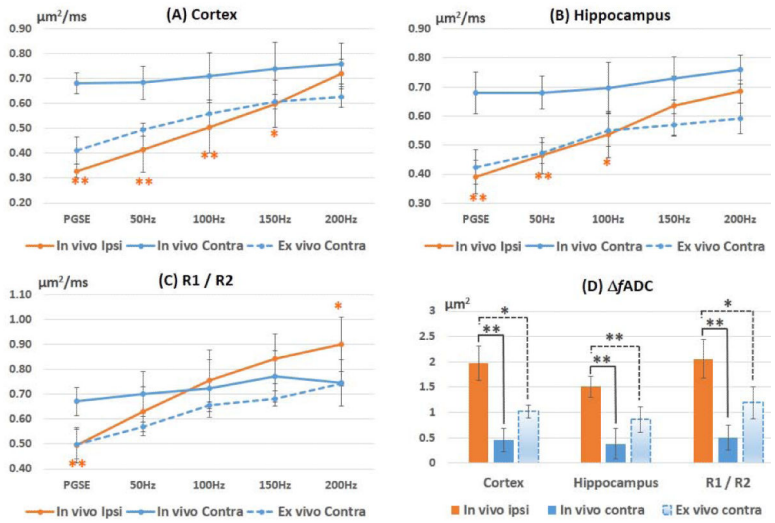

Fig. 4.

Changes in ADC with frequency in the cortex, hippocampus, and the joint regions of the R1 and R2 (R1/R2). The Δ*f*ADC values in the edema regions were significantly higher than both in vivo and ex vivo Δ*f*ADC values measured in the contralateral regions. Error bars indicate the inter-subject standard deviation. The ex vivo ADC values from the ipsilateral side were not included due to large variations (supplemental table 1). * and ** denote that a two-tailed t-test between the ipsilateral and contralateral measurements produced a *p*-value less than 0.01 and 0.001, respectively.

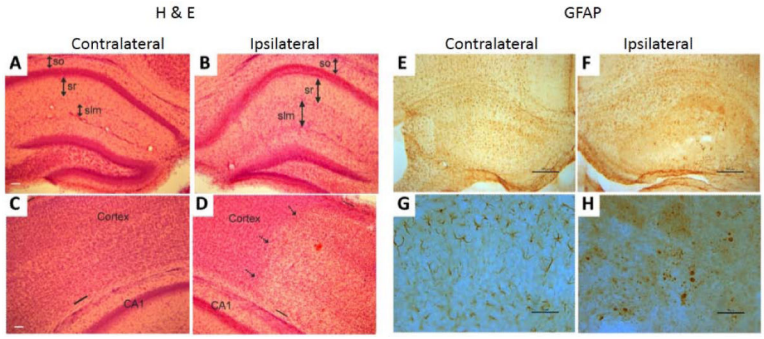

Fig. 5.

H&E and GFAP stained histological sections of the contralateral (control) and ipsilateral (HI) sides of a representative HI injured P11 mouse brain. A-B): In the HI hemisphere (B), severe tissue swelling was found in the hippocampus, with increases in the thickness of the stratum oriens (so), stratum radiatum (sr), and stratum lacunosum/moleculare (slm). Scale bar (in A) = 77 μm (same for B). C-D): Tissue swelling was evident in the cerebral cortex after HI. The dashed arrows indicate the boundary of necrotic region, and the black lines in the pial surface and subcortical white matter indicate the width of cortex. Scale bar (in C) = 77 μm (same for D). E-F: Astrocytic GFAP immunoreactivity (brown staining) was diminished in the HI hippocampus (F) compared to control hippocampus (E). Scale bars (E, F) = 117 μm. G-H: Higher magnification images show normal astrocytes in control hippocampus (G) and fragmented astrocytes in the hippocampus of HI brain (H). Scale bars = 50 μm.

Table 1

In vivo and ex vivo ADC measurements (n=5) of the adult mouse cortex and hippocampus. Data are presented as group mean ± inter-subject standard deviation.

ADC(μm^2/ms)	Cortex		Hippocampus	
	In vivo	Ex vivo	In vivo	Ex vivo
PGSE	0.62±0.02**	0.50±0.01	0.64±0.01**	0.53±0.02
50Hz	0.64±0.02**	0.57±0.02	0.65±0.01**	0.56±0.03
100Hz	0.65±0.02	0.62±0.01	0.67±0.01**	0.60±0.02
150Hz	0.66±0.02	0.65±0.01	0.69±0.01*	0.63±0.02
200Hz	0.69±0.02	0.68±0.02	0.72±0.02*	0.66±0.03
ΔfADC(μm^2)	0.33±0.05**	0.87±0.08	0.38±0.05**	0.66±0.06

Note: * and ** denote that a two-tailed paired t-test between the in vivo and ex vivo measurements produced a *p*-value less than 0.01 and 0.001, respectively.

Table 2

In vivo ADC measurements measured from five P11 mice at 24 hours after hypoxia-ischemia in the cortex, hippocampus, and the two layers of the hippocampus (R1 / R2 as indicated in Fig. C) of the ipsilateral and contralateral hemispheres. Data are shown as group mean ± inter-subject standard deviation.

ADC ($\mu m^2/ms$)	Cortex		Hippocampus		R1/R2	
	Ipsilateral	Contralateral	Ipsilateral	Contralateral	Ipsilateral	Contralateral
PGSE	0.33±0.04**	0.68±0.03	0.39±0.06**	0.68±0.07	0.50±0.07**	0.67±0.06
50Hz	0.41±0.07**	0.68±0.09	0.46±0.06**	0.68±0.06	0.63±0.10	0.70±0.09
100Hz	0.50±0.10**	0.71±0.10	0.54±0.08*	0.70±0.09	0.76±0.12	0.72±0.12
150Hz	0.60±0.11*	0.74±0.10	0.63±0.10	0.73±0.07	0.84±0.10*	0.77±0.10
200Hz	0.72±0.08	0.76±0.06	0.68±0.04	0.76±0.05	0.90±0.11**	0.75±0.09
ΔfADC(μm^2)	1.93±0.36**	0.43±0.24	1.51±0.23**	0.41±0.32	2.05±0.43**	0.44±0.22

Note: * and ** denote that a two-tailed paired t-test between the ipsilateral and contralateral values produced a *p*-value less than 0.01 and 0.001, respectively.